Research Article | Vol. 30, No. 5 / 28 Feb 2022 / Optics Express 6808
Optics EXPRESS

# Visible and near-infrared programmable multi-level diffractive lenses with phase change material $Sb_2S_3$

WEI JIA, RAJESH MENON, AND BERARDI SENSALE-RODRIGUEZ*

*Department of Electrical and Computer Engineering, The University of Utah, Salt Lake City, UT 84112, USA*
*berardi.sensale@utah.edu

**Abstract:** In this paper, we discuss flat programmable multi-level diffractive lenses (PMDL) enabled by phase change materials working in the near-infrared and visible ranges. The high real part refractive index contrast ($\Delta n \sim 0.6$) of $Sb_2S_3$ between amorphous and crystalline states, and extremely low losses in the near-infrared, enable the PMDL to effectively shift the lens focus when the phase of the material is altered between its crystalline and amorphous states. In the visible band, although losses can become significant as the wavelength is reduced, the lenses can still provide good performance as a result of their relatively small thickness ($\sim 1.5\lambda$ to $3\lambda$). The PMDL consists of $Sb_2S_3$ concentric rings with equal width and varying heights embedded in a glass substrate. The height of each concentric ring was optimized by a modified direct binary search algorithm. The proposed designs show the possibility of realizing programmable lenses at design wavelengths from the near-infrared (850 nm) up to the blue (450 nm) through engineering PMDLs with $Sb_2S_3$. Operation at these short wavelengths, to the best of our knowledge, has not been studied so far in reconfigurable lenses with phase-change materials. Therefore, our results open a wider range of applications for phase-change materials, and show the prospect of $Sb_2S_3$ for such applications. The proposed lenses are polarization insensitive and can have the potential to be applied in dual-functionality devices, optical imaging, and biomedical science.



## 1. Introduction

Lenses play an important role in microscopes, cameras, and optical imaging systems, in general. The fixed focal length of a lens limits its practical applications. In recent years, many efforts have been devoted to develop tunable optical lenses through the control of the lens' refractive index and the lens' shape [1] to achieve tunability of the lens' focal length. The tunable light focusing effect of liquid crystal tunable lenses [2] is achieved through an electro-optical effect, which by the way of applying a voltage to change the orientation of the liquid crystals controls its refractive index. On the other hand, devices such as encapsulated fluid-based lenses [3] or elastomeric lenses [4] are designed to have tunable curvature to achieve focal length tuning.

Continued efforts are needed to make programmable lenses with changeable focal length easier to be fabricated. Phase change materials (PCMs) can be good candidates for tunable and programmable lens design due to their large refractive index contrast between their stable phases. As one of the widely used PCMs, vanadium dioxide ($VO_2$) has reversible phase change between metallic and insulating states, but it requires constant energy input to maintain its state [5–7]. Another PCM, $Ge_2Sb_2Te_5$ (GST) has attracted significant attention due to its good stability, large number of switching cycles, fast switching speed, and large refractive index contrast between amorphous and crystalline states [8–14]. Moreover, GST is non-volatile and its state can be maintained without extra power consumption [15]. However, GST has relatively large absorption in both visible and telecommunication wavelengths [15], which limits its application. Recently, a non-volatile material antimony trisulfide ($Sb_2S_3$) emerged as a promising PCM with low losses

#452472 https://doi.org/10.1364/OE.452472
Journal © 2022 Received 28 Dec 2021; revised 5 Feb 2022; accepted 6 Feb 2022; published 15 Feb 2022

Optics EXPRESS

in both amorphous and crystalline states [16,17]. By applying an optical pulse or via thermal heating, the phase of $Sb_2S_3$ can be switched precisely [18]. At wavelength 850 nm, $Sb_2S_3$ has real part of the refractive index contrast ~ 0.6 between its amorphous and crystalline states. Moreover, both states have negligible absorption. The high refractive-index contrast and negligible loss enable $Sb_2S_3$ as a good candidate to design programmable and reconfigurable lenses in the near-infrared.

Metavalent bonded materials, such as GST, are known to be fast crystallizers [19]. Although this enables very fast switching (ns time-scales), it also limits to <100 nm the critical thickness for reversible switching [20]. As a covalently bonded material, the crystallization dynamics of $Sb_2S_3$ are associated with much longer time-scales [19]. Time-scales for crystallization on the order of μs have been recently experimentally verified in several reports [21–22]. Because of this, the critical thickness for reversible switching in $Sb_2S_3$ can be on the order of μm. As a result, development of relatively thick $Sb_2S_3$ metamaterials (>1 μm thickness), as recently proposed in [23–24], is technologically feasible. Such relatively thick metalenses have been demonstrated in other slow crystallizing PCMs such as GSST [20].

Subwavelength structures have been applied to design varifocal metalenses with phase change material $Sb_2S_3$ at a near-infrared wavelength of $\lambda$ = 1310nm [24]. However, these proposed metalenses require subwavelength lateral feature sizes, and are part of a multilayered structure, thus can be complicated to fabricate. Furthermore, because of the physical origin of the diffractive power, these lenses are polarization sensitive, and it is not clear whether operation at shorter wavelengths (where losses are higher) is possible. It is to be mentioned that visible-band $Sb_2S_3$ meta-displays have also been recently demonstrated [22]. Here, we present the design of a flat, programmable multi-level diffractive lens (PMDL) using $Sb_2S_3$. Fixed focus multi-level diffractive lenses (MDLs), without PCM, have been experimentally demonstrated [25–27]. The proposed PMDL design with PCM $Sb_2S_3$ can have feature sizes greater than 3λ, and it can be polarization insensitive, which is crucial for general-purpose imaging. The PMDL with PCM consists of $Sb_2S_3$ concentric rings with identical widths embedded in a glass substrate (see Fig. 1). The height of each $Sb_2S_3$ concentric ring is optimized through a modified direct binary search algorithm. At amorphous state, the focal length of PMDL is $f_{amor}$. After switching $Sb_2S_3$ from amorphous state to crystalline state, the focal length of the PMDL changes to $f_{crys}$. Through

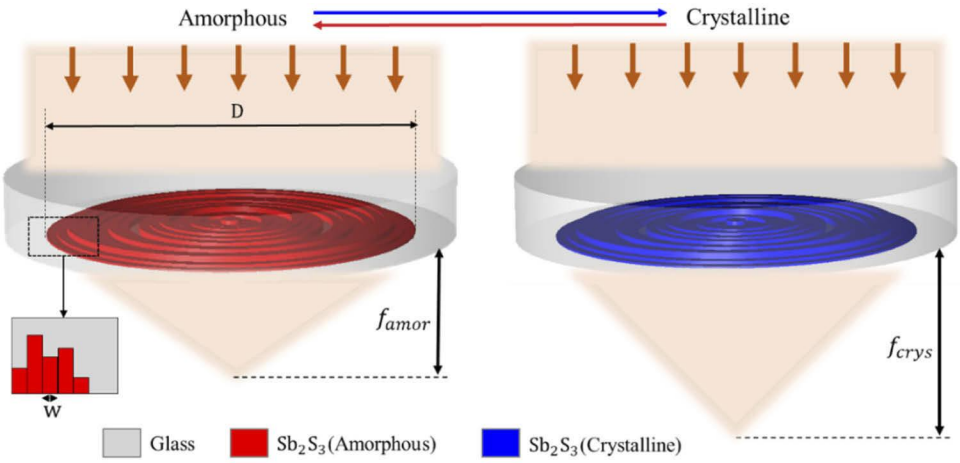


**Fig. 1.** Schematic of the programmable multi-level diffractive lens with $Sb_2S_3$. The PMDL has focal length $f_{amor}$ with amorphous state of $Sb_2S_3$, and focal length $f_{crys}$ with crystalline state of $Sb_2S_3$.

Optics EXPRESS

this approach, we show lenses operating not only in the near-infrared, but also at several design wavelengths across the whole visible spectrum (red to blue). The main contributions of this work are two-fold. For one, we introduce PMDLs by merging the concept of inverse-designed MDLs with phase change materials. This is something uniquely enabled by slow-crystallizing PCMS such as $Sb_2S_3$, $Sb_2Se_3$, GSST, etc., wherein reversible switching of structures on the order or thicker than a wavelength is possible. For two, we show for the first time, to the best of our knowledge, the possibility of realizing programmable lenses in the visible enabled by PCMs by taking advantage of the low-loss of $Sb_2S_3$, which makes it a revolutionary PCM for reconfigurable applications at these short wavelengths.

## 2. PMDL device design

The schematic of the programmable multi-level diffractive lens is shown in Fig. 1. The PMDL has diameter, D and consists of $Sb_2S_3$ concentric rings with identical width, W embedded in the glass substrate. The heights of the $Sb_2S_3$ concentric rings in each design varies from 0 to H with total height levels N, resulting in a step height size $\Delta h = H/(N-1)$. The refractive index of the glass substrate is shown in Fig. 2(a), which is extracted from Ref. [28]. The glass substrate has no loss in the visible and near-infrared wavelength range. Refractive index value 1.4525 is used in the optimization at wavelength 850 nm for the glass substrate. The complex refractive indices of amorphous and crystalline states of $Sb_2S_3$ are extracted from Ref. [18], and depicted in Figs. 2(b)–2(c). Refractive index values $n_{amor} = 2.9129 + j0.0000$ and $n_{crys} = 3.5568 + j0.0000$ are used in the optimization at wavelength 850 nm. It is to note that the imaginary part of refractive index is $<10^{-5}$ at this wavelength. Scalar diffraction theory in the regime of Fresnel approximation is used to simulate the lens [29]. The height distribution of the $Sb_2S_3$ concentric rings is optimized during lens design. In the amorphous state of $Sb_2S_3$, the focal length of the PMDL is $f_{amor}$. As $Sb_2S_3$ transitions to crystalline state through heating, the focal length of the PMDL shifts to $f_{crys}$. The PMDL design parameters are shown in Table 1. For broadband optimization, dispersion is considered for both glass substrate and $Sb_2S_3$. The refractive index values used for $Sb_2S_3$ in the amorphous state at visible wavelengths 650, 550 and 450 nm are $3.1113 + j0.0000$, $3.4321 + j0.1329$, and $3.6627 + j0.7437$, respectively. Refractive index values $3.9492 + j0.2260$, $4.1584 + j0.6389$, and $4.1043 + j1.4191$ are used for $Sb_2S_3$ in the crystalline state at the visible wavelengths of 650, 550 and 450 nm, respectively. The corresponding refractive index values used at these wavelengths for glass substrate are 1.4565, 1.4599 and 1.4656.

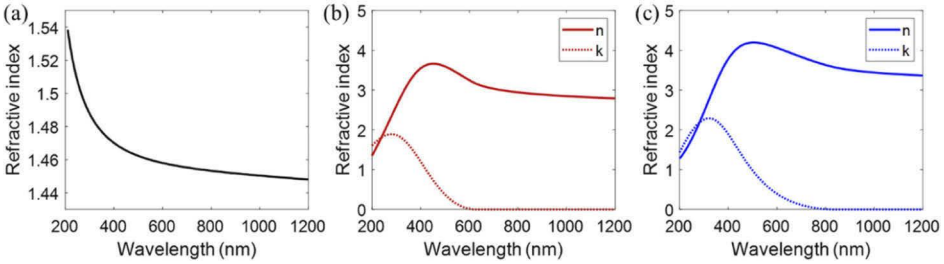


**Fig. 2.** (a) Refractive index of fused silica glass (data extracted from [26]). Complex refractive index of $Sb_2S_3$ in the (b) amorphous state, and (c) crystalline state (data extracted from [18]).

A modified direct binary search algorithm is performed to optimize the height distribution of the $Sb_2S_3$ concentric rings, as illustrated in Fig. 3. A randomly generated height distribution is used as the initial height distribution. Then, the initial figure-of-merit (FOM) is calculated. The FOM defined here for amorphous and crystalline state of $Sb_2S_3$ follows the definition used in Ref. [30]. And the averaged FOM ($(FOM_{amor} + FOM_{crys})/2$) is used after calculating the FOM

Optics EXPRESS

**Table 1. Programmable MDL designs.**

| Designs | $\lambda$ ($nm$) | W ($\mu$m) | D (mm) | H(μm) | N | $f_{amor}$ (mm) | $f_{crys}$ (mm) |
|---|---|---|---|---|---|---|---|
| PMDL 1 | 850 | 1 | 0.2 | 2 | 41 | 0.4 | 0.5 |
| PMDL 2 | 850 | 3 | 1.2 | 2 | 41 | 10 | 15 |
| PMDL 3 | 800 ~ 900 | 3 | 1.2 | 2 | 41 | 10 | 15 |
| PMDL 4 | 650 | 3 | 1.2 | 0.6 | 41 | 10 | 15 |
| PMDL 5 | 550 | 3 | 1.2 | 0.6 | 41 | 10 | 15 |
| PMDL 6 | 450 | 3 | 1.2 | 0.5 | 26 | 10 | 15 |

of each state. As for broadband design, the FOM is obtained by averaging FOMs obtained at each wavelength. In one iteration, all ring height are perturbed in a random sequence manner. After selecting a ring, the randomly generated height, $\Delta h \times N_r$ ($\Delta h$ is the step height, and $N_r$ is the random integer in [0, N-1]) is applied to the selected ring. If the new calculated FOM is increased, then the height is kept, otherwise the initial height is retained. Then, it proceeds to the next ring. One iteration ends when all the rings are traversed. The convergence of the algorithm can be guaranteed by a termination condition, which can be defined as the minimum FOM difference between two consecutive iterations or by imposing a maximum number of total iterations. Here, the minimum FOM difference is set to be zero and maximum number of total iterations is set to be 500. The optimized height distribution of the $Sb_2S_3$ concentric rings is obtained once the termination condition is met. The simulations and optimizations were carried out in MATLAB and each iteration only takes a few seconds to finish, due to the small dimension of the problem, using a personal computer with 6 Intel Core i7-8700U CPU at 3.20 GHz, and 16 GB installed RAM.

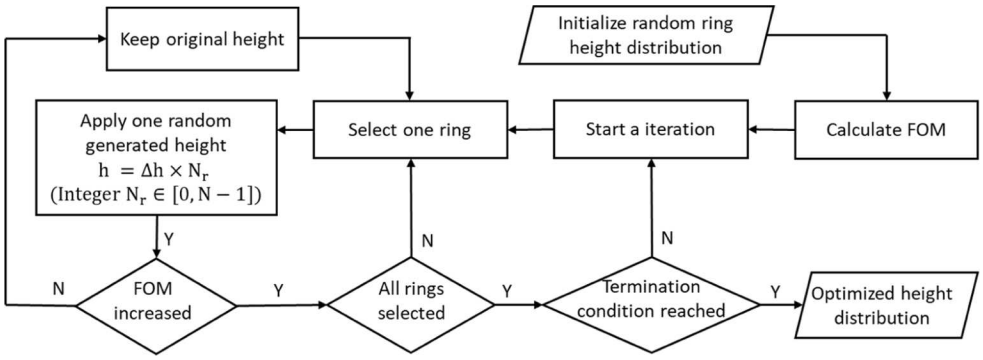


**Fig. 3.** Flowchart of the optimization algorithm used in determining the height distribution of the $Sb_2S_3$ concentric rings.

## 3. Results and discussion

The focusing performance of the PMDL is characterized by simulating the point-spread functions (PSFs) and evaluating the full-width-at-half-maximum (FWHM) in each state. The target PSF in the optimization is chosen to be a diffraction-limited Gaussian with FWHM = $\lambda/(2NA)$. NA is the numerical aperture and is determined by $sin(tan^{-1}(D/2f))$. The PMDL 1 design has diameter 0.2 mm, focal length 0.4 mm in the amorphous state, and 0.5 mm in the crystalline state. The calculated NA for PMDL 1 design is 0.2425 in the amorphous state, and 0.1961 in the crystalline state. For PMDL 1 design, in the amorphous state, the simulated 2D on-axis PSF on the focal plane is shown in Fig. 4(a), and its corresponding normalized on-axis intensity distribution in the

Optics EXPRESS

lateral direction is shown in Fig. 4(b). The FWHM obtained after optimization is 1.82 $\mu$m in the amorphous state. The intensity distribution after transmitting through the PMDL on the x-z plane is shown in Fig. 4(c). It shows that the transmitted light is focused tightly at 0.4 mm as desired. The 2D on-axis PSF on focal plane in the crystalline state is shown in Fig. 4(d). As $Sb_2S_3$ transitioned to the crystalline state, the FWHM is increased to 2.21 $\mu$m, as shown in Fig. 4(e), as expected from the increased focal length 0.5 mm (and correspondingly decreased NA) in the crystalline state. The obtained FWHMs, 1.82 and 2.21 $\mu$m are close to the diffraction limited FWHMs, 1.75 and 2.17 $\mu$m calculated by $\lambda/(2NA)$. The light distribution on the x-z plane in Fig. 4(f) confirms that the focal length of the PMDL shifts to 0.5 mm as $Sb_2S_3$ transitioned to the crystalline state.

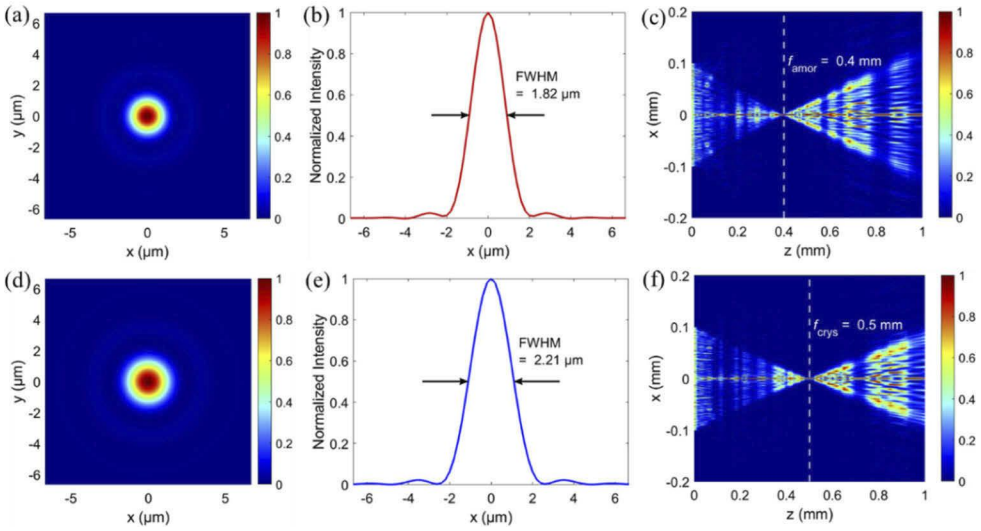


**Fig. 4.** PMDL 1 with $Sb_2S_3$ in the amorphous state: (a) 2D PSF, (b) 1D PSF across the middle, and (c) light distribution on the x-z plane. For $Sb_2S_3$ in the crystalline state: (d) 2D PSF, (e) 1D PSF across the middle, and (f) light distribution on the x-z plane.

The optimized height distribution of the $Sb_2S_3$ concentric rings for PMDL 1 is shown in Fig. 5(a). The light grey color indicates glass substrate, and the red color represents $Sb_2S_3$. The optimized height is imported to commercial finite element software COMSOL Multiphysics for further verification. The electric field distributions of PMDL 1 on the x-z plane of the amorphous and crystalline are shown in Figs. 5(b) and 5(c). It can be clearly observed that the focal length is 0.4 mm in the amorphous state, and the focal length of PMDL 1 shifts to 0.5 mm as $Sb_2S_3$ transitioned to the crystalline state. The simulated focal length for both states match well with the results obtained from the scalar diffraction theory, which confirms and validates the design.

Compared to PMDL 1, PMDL 2 has larger diameter of 1.2 mm and larger focal length for both states. The focal length in the amorphous state is 10 mm, and 15 mm in the crystalline state. The resulting NAs are 0.06 and 0.04 for amorphous and crystalline states, respectively. The 2D on-axis PSF in the amorphous and in the crystalline states are shown in Figs. 6(a) and 6(d). From Fig. 6(b), the FWHM is 7.34 $\mu$m in the amorphous state. In the crystalline state, the FWHM increased to 11.03 $\mu$m, as shown in Fig. 6(e). The simulated FWHMs are close to the diffraction limit of 7.10 and 10.63 $\mu$m, respectively. The x-z plane light distribution shown in Figs. 6(c) and 6(f) confirm that PMDL 2 has focal length 10 mm in the amorphous state, and 15 mm in the crystalline state, as desired.

Based on the proposed PMDL concept, it is possible to realize reconfigurable lenses operating across broadband wavelength ranges. The design of a broadband PMDL is shown in PMDL 3.

Optics EXPRESS

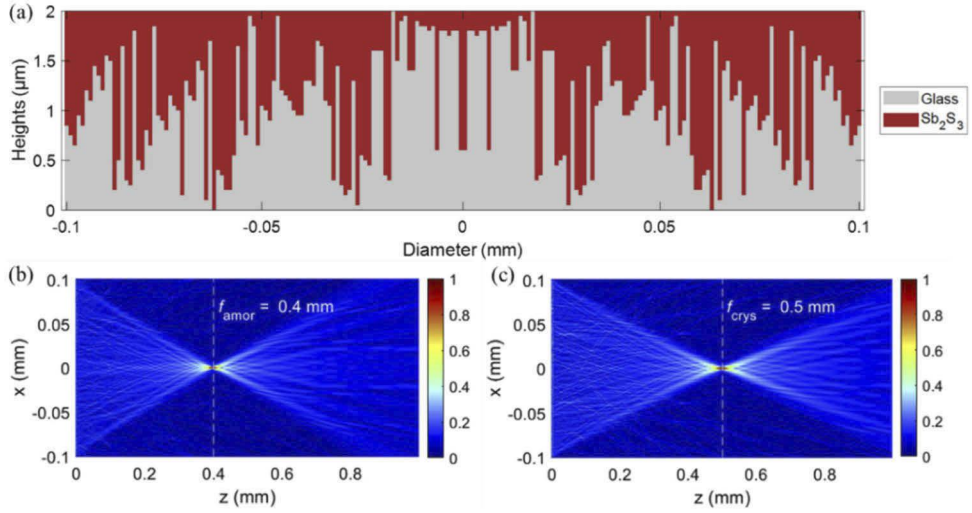


**Fig. 5.** (a) PMDL 1: height distribution of glass and $Sb_2S_3$. Electric field distribution on x-z plane with $Sb_2S_3$ at (b) amorphous state, and (c) crystalline state (finite element simulations).

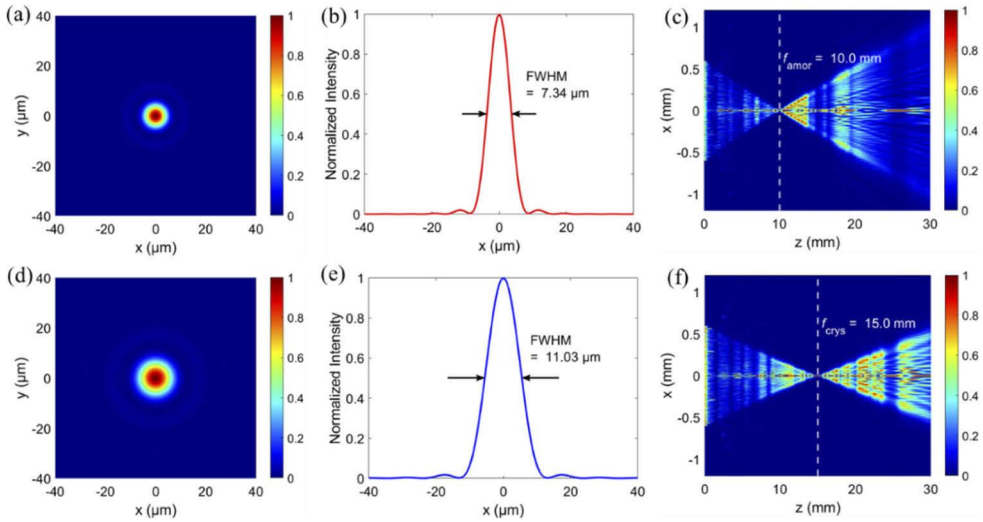


**Fig. 6.** PMDL 2 with $Sb_2S_3$ in the amorphous state: (a) 2D PSF, (b) 1D PSF across the middle, and (c) light distribution on the x-z plane. For $Sb_2S_3$ in the crystalline state: (d) 2D PSF, (e) 1D PSF across the middle, and (f) light distribution on the x-z plane.

The PMDL 3 has the same diameter and focal lengths as PMDL 2. The PMDL 3 has a 100 nm bandwidth, that is from 800 nm to 900 nm. During design, a wavelength sampling of 25 nm was employed. Shown in Fig. 7 are the PSFs for PMDL 3. The obtained FWHMs are 7.79, 14.04, 13.20, 10.70, and 8.28 $\mu$m at $\lambda = 800$, 825, 850, 875, and 900 nm in the amorphous state with focal length, 10 mm. In the crystalline state, as shown in Fig. 8, the FWHMs are 11.14, 12.81, 15.09, 12.80, 12.25 $\mu$m at $\lambda = 800$, 825, 850, 875, and 900 nm with focal length, 15 mm.

Moreover, we also demonstrated that the proposed reconfigurable PMDL can work in the visible wavelength range. Three lenses, designed for $\lambda = 650$, 550, and 450 nm, respectively, are

Optics EXPRESS

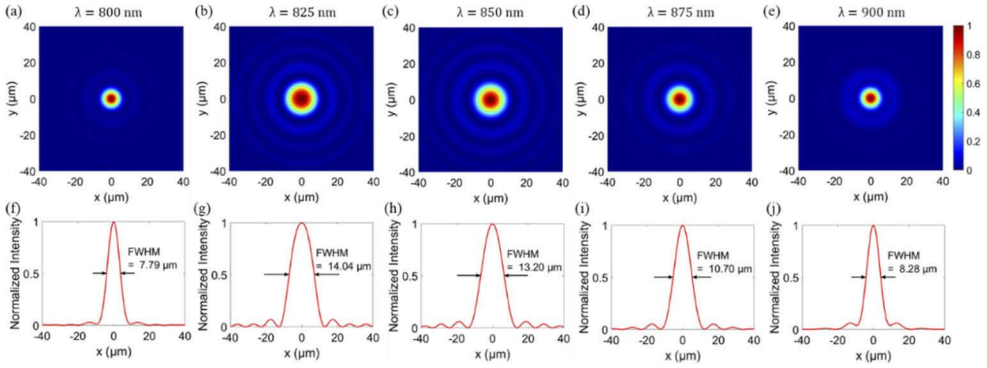


**Fig. 7.** PMDL 3 (broadband lens) in the amorphous state with focal length 10 mm on the focal plane: 2D PSF at wavelength (a) 800nm, (b) 825 nm, (c) 850 nm, (d) 875 nm, (e) 900 nm, and 1D PSF across the middle at wavelength (f) 800 nm, (g) 825 nm, (h) 850 nm, (i) 875 nm, (j) 900 nm.

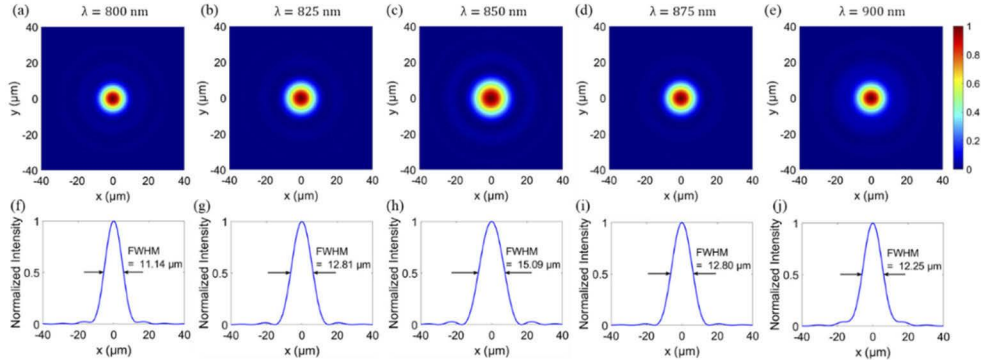


**Fig. 8.** PMDL 3 (broadband lens) in the crystalline state with focal length 15 mm on the focal plane: 2D PSF at wavelength (a) 800nm, (b) 825 nm, (c) 850 nm, (d) 875 nm, (e) 900 nm, and 1D PSF across the middle at wavelength (f) 800 nm, (g) 825 nm, (h) 850 nm, (i) 875 nm, (j) 900 nm.

shown in PMDL 4, 5, and 6. All three PMDLs have same diameter, 1.2 mm and same focal lengths, which are 10 mm in the amorphous state, and 15 mm in the crystalline state. PMDL 4 and PMDL 5 have the same height range 0 to 0.6 $\mu$m, and same number of height levels of 41. For PMDL 6, the height range is 0 to 0.5 $\mu$m, and the number of height levels is 26. The reduced maximum height used for PMDL 4, 5, 6 are due to the loss introduced in the $Sb_2S_3$ material at these shorter wavelengths. The simulated 2D on-axis PSFs and their corresponding normalized on-axis intensity distributions for PMDLs 4, 5 and 6 are shown in Fig. 9. The FWHMs in the amorphous state are 5.65, 4.79, and 3.89 $\mu$m at $\lambda = 650$, 550, and 450 nm, respectively, which are close to the diffraction limited FWHMs of 5.43, 4.59 and 3.76 $\mu$m. The FWHM gets smaller as the wavelength decreases. In the crystalline state, the obtained FWHMs are 8.38, 7.07, and 6.08 $\mu$m at wavelengths 650, 550, and 450 nm, respectively. Compared to the diffraction limited FWHMs of 8.13, 6.88 and 5.63 in the crystalline state, the differences are small. It is noted in Figs. 9(i)–9(l) for the lens designed at wavelength 450 nm, that some sidelobes are observed, which might be attributed to the losses of $Sb_2S_3$ in both states. It is to be noticed that at shorter wavelengths, absorption in $Sb_2S_3$ becomes significant. Even though a lens design is proposed at 450 nm, this lens has a very poor transmission efficiency.

Optics EXPRESS

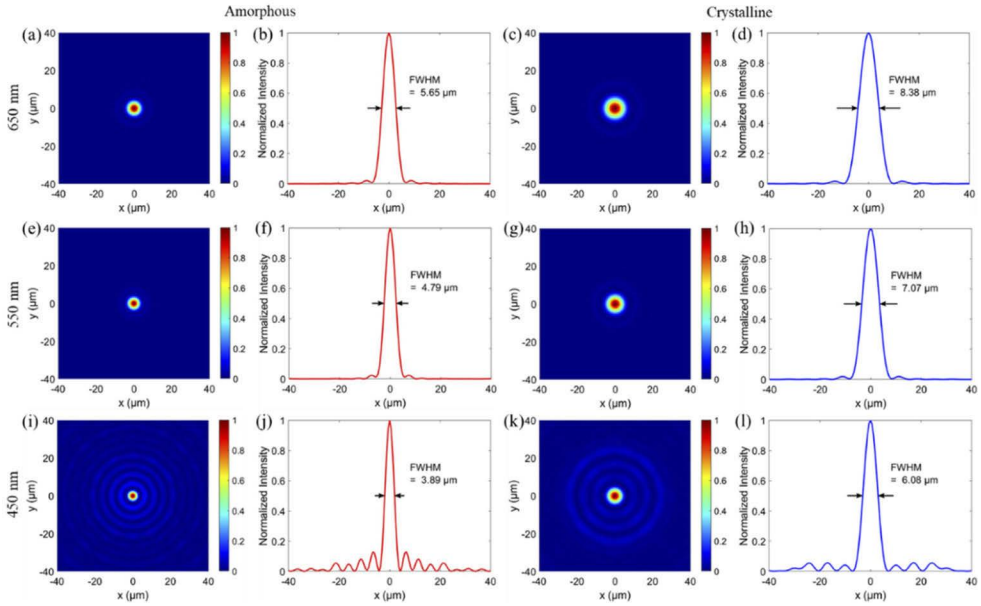


**Fig. 9.** PMDL 4 (at 650 nm) in the amorphous state: (a) 2D PSF, (b) 1D PSF across the middle, and in the crystalline state: (c) 2D PSF, (d) 1D PSF across the middle. PMDL 5 (at 550 nm) in the amorphous state: (e) 2D PSF, (f) 1D PSF across the middle, and in the crystalline state: (g) 2D PSF, (h) 1D PSF across the middle. PMDL 6 (at 450 nm) in the amorphous state: (i) 2D PSF, (j) 1D PSF across the middle, and in the crystalline state: (k) 2D PSF, (l) 1D PSF across the middle.

The fabrication of the proposed PMDL with phase change material $Sb_2S_3$ can be as follows: first, multiple etching steps are to be performed in the glass substrate to obtain the desired depths. Then sputtering the $Sb_2S_3$ material on top of the etched glass substrate. Followed by polishing the top surface or annealing to get the uniform $Sb_2S_3$ material distribution and deposition of a thin capping layer. Owing to the ease of fabrication of these PMDLs compared to metalenses and conventional refractive lenses, this demonstration will play an important role in programmable lens designs. Multiphysics simulations, performed in COMSOL (using the same formalisms as in [31]), show that it is possible to program the lenses herein proposed (switching from crystalline to amorphous state) by raster-scanning a laser beam (see Supplement 1 for further details). Such a mechanism has been experimentally shown in thinner films e.g. [32–33]. Our simulation results predict that long laser pulses (hundred nanosecond scale) enable heating up a wide cross-sectional volume as heat diffuses laterally from the center of the focal spot. However, the temperature relaxation dynamics in this case are relatively slow. Once that the laser pulse ends, the maximum temperature drops below crystallization temperature in 100's of ns. In order for the whole volume to undergo complete phase transition, because of the relatively large thickness of the proposed lenses, laser wavelengths associated with low absorption coefficient in crystalline state should be employed (i.e., $\lambda > 800$ nm). Consequently, high-power pulses are also required so to induce sufficient heating so as to reach a temperature above the $Sb_2S_3$ melting (~550°C) across the whole film. In the other hand, by using a train of short pulses (fs to ns duration) rather than one pulse, and by selecting the laser wavelength so that absorption could happen over a characteristic length on the order of ~100 nm (e.g., $\lambda = 580$ nm), an even faster temperature relaxation (on the order of 10 ns) might be possible. In this case, the first pulse amorphizes the top volume of the film and each subsequent pulse transmits with little attenuation through the area already

Optics EXPRESS

amorphized. Each subsequent pulse is absorbed deeper in the film. Therefore, deeper and deeper volumes are amorphized with each new arriving pulse. The number of pulses to be applied is dictated by the thickness of the lens (e.g., whereas a 500 nm thickness might require 5-6 pulses, a 2 μm thickness might require >20 pulses). The opposite process, switching the lenses from amorphous to crystalline state, can be simply attained by heating so as to reach the crystallization temperature of $Sb_2S_3$ (~270°C).

## 4. Conclusion

We propose the use of $Sb_2S_3$ to modulate the focal length (i.e., programmable) of flat multi-level diffractive lenses in the visible to near-infrared bands. The proposal is supported by six numerically optimized designs of such PMDLs and their corresponding simulations. Both narrowband and broadband PMDLs are possible with close to diffraction-limited focusing. The high real part refractive index contrast ($\Delta n \sim 0.6$) of $Sb_2S_3$ between amorphous and crystalline states and zero losses at wavelength 850 nm enable the programmable MDL to shift the focal length between its two states with high focusing efficiency. The heights of $Sb_2S_3$ concentric rings vary from 0 to 2 μm with step size 50 nm for the design at wavelength 850 nm. The NAs are 0.06 in the amorphous state and 0.04 in the crystalline state. FWHMs obtained from simulation is 7.34 $\mu$m in the amorphous states, at 11.03 $\mu$m in the crystalline state, which are close to the diffraction limits 7.10 and 10.63 $\mu$m. By switching $Sb_2S_3$ from amorphous state to crystalline state, the focal length of the MDL changes from 10 mm to 15 mm. Furthermore, PMDL working at 650, 550, and 450 nm are also demonstrated in this paper. The proposed polarization insensitive PMDL can be easier to manufacture compared to metalenses, and it has the potential to be applied in many areas, such as dual-functional devices, optical imaging, and biomedical science.

**Funding.** National Science Foundation (ECCS #1936729).

**Disclosures.** The authors declare no conflict of interest.

**Data availability.** Data underlying the results presented in this paper are not publicly available at this time but may be obtained from the authors upon reasonable request.

**Supplemental document.** See Supplement 1 for supporting content.

## References

1. L. Chen, M. Ghilardi, J. J. C. Busfield, and F. Carpi, "Electrically Tunable Lenses: A Review," Front. Robot. AI **8**, 166 (2021).
2. Y.-H. Lin, Y.-J. Wang, and V. Reshetnyak, "Liquid crystal lenses with tunable focal length," Liq. Cryst. Rev. **5**(2), 111–143 (2017).
3. N. Hasan, A. Banerjee, H. Kim, and C. H. Mastrangelo, "Tunable-focus lens for adaptive eyeglasses," Opt. Express **25**(2), 1221–1233 (2017).
4. S. Liu, Y. Qiu, and W. Yu, "Self-Contained Focus-Tunable Lenses Based on Transparent and Conductive Gels," Macromol. Mater. Eng. **305**(11), 2000393 (2020).
5. M. Mao, Y. Liang, R. Liang, L. Zhao, N. Xu, J. Guo, F. Wang, H. Meng, H. Liu, and Z. Wei, "Dynamically Temperature-Voltage Controlled Multifunctional Device Based on VO2 and Graphene Hybrid Metamaterials: Perfect Absorber and Highly Efficient Polarization Converter," Nanomater. **9**, 1 (2019).
6. S. Cueff, J. John, Z. Zhang, J. Parra, J. Sun, R. Orobtchouk, S. Ramanathan, and P. Sanchis, "VO2 nanophotonics," APL Photonics **5**(11), 110901 (2020).
7. K. J. Miller, K. A. Hallman, R. F. Haglund, and S. M. Weiss, "Silicon waveguide optical switch with embedded phase change material," Opt. Express **25**(22), 26527–26536 (2017).
8. Q. Wang, E. T. F. Rogers, B. Gholipour, C.-M. Wang, G. Yuan, J. Teng, and N. I. Zheludev, "Optically reconfigurable metasurfaces and photonic devices based on phase change materials," Nat. Photonics **10**(1), 60–65 (2016).
9. A.-K. U. Michel, M. Wuttig, and T. Taubner, "Design Parameters for Phase-Change Materials for Nanostructure Resonance Tuning," Adv. Opt. Mater. **5**(18), 1700261 (2017).
10. J. W. Park, S. H. Eom, H. Lee, J. L. F. Da Silva, Y. S. Kang, T. Y. Lee, and Y. H. Khang, "Optical properties of pseudobinary GeTe, Ge2 Sb2 Te5, GeSb2 Te4, GeSb4 Te7, and Sb2 Te3 from ellipsometry and density functional theory," Phys. Rev. B: Condens. Matter Mater. Phys. **80**(11), 115209 (2009).
11. A. Karvounis, B. Gholipour, K. F. MacDonald, and N. I. Zheludev, "All-dielectric phase-change reconfigurable metasurface," Appl. Phys. Lett. **109**(5), 051103 (2016).

Optics EXPRESS


12. J. Zhang, Y. Zhang, Q. Hong, W. Xu, Z. Zhu, and X. Yuan, "Near-Infrared Rewritable, Non-Volatile Subwavelength Absorber Based on Chalcogenide Phase Change Materials," Nanomaterials **10**(6), 1222 (2020).
13. J. Tian, Q. Li, J. Lu, and M. Qiu, "Reconfigurable all-dielectric antenna-based metasurface driven by multipolar resonances," Opt. Express **26**(18), 23918–23925 (2018).
14. T. Cao, K. Liu, Y. Tang, J. Deng, K. Li, and G. Li, "A High-Index Ge2Sb2Te5-Based Fabry–Perot Cavity and Its Application for Third-Harmonic Generation," Laser Photon. Rev. **13**(7), 1900063 (2019).
15. S. Abdollahramezani, O. Hemmatyar, H. Taghinejad, A. Krasnok, Y. Kiarashinejad, M. Zandehshahvar, A. Alù, and A. Adibi, "Tunable nanophotonics enabled by chalcogenide phase-change materials," Nanophotonics **9**(5), 1189–1241 (2020).
16. K. V. Sreekanth, Q. Ouyang, S. Sreejith, S. Zeng, W. Lishu, E. Ilker, W. Dong, M. ElKabbash, Y. Ting, C. T. Lim, M. Hinczewski, G. Strangi, K.-T. Yong, R. E. Simpson, and R. Singh, "Phase-Change-Material-Based Low-Loss Visible-Frequency Hyperbolic Metamaterials for Ultrasensitive Label-Free Biosensing," Adv. Opt. Mater. **7**(12), 1900081 (2019).
17. W. Dong, H. Liu, J. K. Behera, L. Lu, R. J. H. Ng, K. V. Sreekanth, X. Zhou, J. K. W. Yang, and R. E. Simpson, "Wide Bandgap Phase Change Material Tuned Visible Photonics," Adv. Funct. Mater. **29**(6), 1806181 (2019).
18. M. Delaney, I. Zeimpekis, D. Lawson, D. W. Hewak, and O. L. Muskens, "A New Family of Ultralow Loss Reversible Phase-Change Materials for Photonic Integrated Circuits: Sb2S3 and Sb2Se3," Adv. Funct. Mater. **30**(36), 2002447 (2020).
19. M.J. Müller, A. Yadav, C. Persch, S. Wahl, F. Hoff, and M. Wuttig, "Tailoring Crystallization Kinetics of Chalcogenides for Photonic Applications," Adv. Electron. Mater. **11**, 2100974 (2021).
20. M. Y. Shalaginov, S. An, Y. Zhang, F. Yang, P. Su, V. Liberman, J. B. Chou, C. M. Roberts, M. Kang, C. Rios, Q. Du, C. Fowler, A. Agarwal, K. A. Richardson, C. Rivero-Baleine, H. Zhang, J. Hu, and T. Gu, "Reconfigurable all-dielectric metalens with diffraction-limited performance," Nat. Commun. **12**(1), 1225 (2021).
21. Z. Fang, J. Zheng, A. Saxena, J. Whitehead, Y. Chen, and A. Majumdar, "Non-Volatile Reconfigurable Integrated Photonics Enabled by Broadband Low-Loss Phase Change Material," Adv. Opt. Mater. **9**(9), 2002049 (2021).
22. O. Hemmatyar, S. Abdollahramezani, S. Lepeshov, A. Krasnok, T. Brown, A. Alu, and A. Adibi, "Advanced Phase-Change Materials for Enhanced Meta-Displays," arXiv Prepr. arXiv:2105.01313 (2021).
23. Y. Wang, L. Chen, S. Tang, P. Xu, F. Ding, Z. Fang, and A. Majumdar, "Helicity-dependent continuous varifocal metalens based on bilayer dielectric metasurfaces," Opt. Express **29**(24), 39461–39472 (2021).
24. S. Qin, N. Xu, H. Huang, K. Jie, H. Liu, J. Guo, H. Meng, F. Wang, X. Yang, and Z. Wei, "Near-infrared thermally modulated varifocal metalens based on the phase change material Sb2S3," Opt. Express **29**(5), 7925–7934 (2021).
25. M. Meem, S. Banerji, C. Pies, T. Oberbiermann, A. Majumder, B. Sensale-Rodriguez, and R. Menon, "Large-area, high-numerical-aperture multi-level diffractive lens via inverse design," Optica **7**(3), 252–253 (2020).
26. S. Banerji, M. Meem, A. Majumder, F. G. Vasquez, B. Sensale-Rodriguez, and R. Menon, "Imaging with flat optics: metalenses or diffractive lenses?" Optica **6**(6), 805–810 (2019).
27. S. Banerji, M. Meem, A. Majumder, B. Sensale-Rodriguez, and R. Menon, "Extreme-depth-of-focus imaging with a flat lens," Optica **7**(3), 214–217 (2020).
28. I. H. Malitson, "Interspecimen Comparison of the Refractive Index of Fused Silica*,†," J. Opt. Soc. Am. **55**(10), 1205–1209 (1965).
29. X. Wan, B. Shen, and R. Menon, "Diffractive lens design for optimized focusing," J. Opt. Soc. Am. A **31**(12), B27–B33 (2014).
30. P. Wang, N. Mohammad, and R. Menon, "Chromatic-aberration-corrected diffractive lenses for ultra-broadband focusing," Sci. Rep. **6**(1), 21545 (2016).
31. D. Lawson, D.W. Hewak, O.L. Muskens, and I. Zeimpekis, "Time-resolved reversible optical switching of the ultralow-loss phase change material Sb2Se3," arXiv preprint arXiv:2111.13182 (2021).
32. H. Liu, W. Dong, H. Wang, L. Lu, Q. Ruan, Y.S. Tan, R.E. Simpson, and J.K. Yang, "Rewritable color nanoprints in antimony trisulfide films," Sci. Adv. **6**(51), eabb7171 (2020).
33. K. Gao, K. Du, S. Tian, H. Wang, L. Zhang, Y. Guo, B. Luo, W. Zhang, and T. Mei, "Intermediate Phase-Change States with Improved Cycling Durability of Sb2S3 by Femtosecond Multi-Pulse Laser Irradiation," Adv. Funct. Mater. **31**(35), 2103327 (2021).